

Suzaku Observation of Abell 1555 and Abell 1558: Searching for Non-thermal Emission from Large Scale Structure Formation

Ryu MAKIYA, Tomonori TOTANI

Dept. of Astronomy, Kyoto University, Kitashirakawa-Oiwake-cho, Sakyo-ku, Kyoto 606-8502
makiya@kusastro.kyoto-u.ac.jp, totani@kusastro.kyoto-u.ac.jp

Kazuhiro NAKAZAWA

Department of Physics, The University of Tokyo, 7-3-1Hongo, Bunkyo-ku, Tokyo 113-0033
nakazawa@amalthaea.phys.s.u-tokyo.ac.jp

(Received 2000 December 31; accepted 2001 January 1)

Abstract

We report X-ray observations of two galaxy clusters Abell 1555 and Abell 1558 with *Suzaku*, which are included in a large scale filamentary structure and a supercluster, to search for non-thermal emission driven by shocks produced in structure formation. These two clusters are detected by *Suzaku*/XIS for the first time in the X-ray band of 0.5–7 keV. No significant flux is detected by HXD in the energy band of 13–40 keV, and upper limits are reported. From the analysis of the XIS data, we find that the spectrum of A1555 is fit by a thermal plus power-law model, significantly better than a single-temperature pure thermal spectrum. If this power-law component is due to inverse-Compton scattering, the fraction of total baryon energy imparted to non-thermal electrons is consistent with the typical value inferred from the observation of other clusters. However, other scenarios (e.g., under lying AGNs, multi-temperature thermal models) cannot be excluded and further investigation of this system is desired. Basic physical properties of A1555 (e.g., total mass) are also reported.

Key words: X-rays: galaxies: clusters: individual (Abell 1555): individual (Abell 1558): non-thermal

1. Introduction

Galaxy clusters are the largest gravitationally bound structures in the Universe. It contains $\sim 10^{15} M_{\odot}$ hot gas, galaxies, dark matter, and non-thermal components such as magnetic fields and cosmic-rays. Although the detailed properties of galaxy clusters are intrinsically interesting topics, they are also important to understand the formation and evolution of the large scale structure, and acceleration mechanisms of cosmic-rays.

According to the cold dark matter scenario, which is the most successful theory of the structure formation, structures grow up hierarchically from small scale to large scale. When an object collapses gravitationally and virializes, shock waves occurs and a fraction of the baryonic matters in objects are accelerated into relativistic energies, if the shock waves are strong enough. Accelerated electrons scatter the Cosmic Microwave Background (CMB) photons up to hard X-ray and gamma-ray regions via the Inverse-Compton (IC) mechanism (for a recent review of gamma-rays from structure formation, see Blasi et al. 2007).

Although the IC emission due to the structure formation has not been detected at high significance, the existence of relativistic electrons in several clusters has been revealed by the observations of diffuse radio emission from galaxy clusters (Willson 1970; Giovannini & Feretti 2000; Govoni & Feretti 2004; Feretti 2005). These extended radio emissions are called as “radio halos”, which is located at the cluster center, or “radio relics” at the cluster periph-

ery. They have steep spectra and a cutoff at a few GHz, implying that the relativistic electrons account for the radio emission. The radio halos or relics are found in the merging clusters, and hence these electrons are considered to be accelerated in the cosmological shock waves.

Since cluster X-ray emission is dominated by a thermal component below ~ 20 keV and expected non-thermal emission has a low flux, observing the IC emission is a difficult task. Although great effort has been devoted to search for the non-thermal IC emission, results are still controversial. For example, Beppo SAX reported the detection of hard X-ray emission from Coma cluster (Fusco-Femiano et al. 1999; Fusco-Femiano et al. 2004), but these detections are still a matter of debate (Rossetti & Molendi 2004; Fusco-Femiano et al. 2007). Observations of galaxy clusters in gamma-ray band have also been performed by ground-based air Cherenkov telescopes and *Fermi* (e.g., Aharonian et al. 2009a; Aharonian et al. 2009b; Aleksic et al. 2010; Ackermann et al. 2010), but no significant detection of non-thermal emission has been achieved, only resulting in flux upper limits.

Here we report X-ray observations of two galaxy clusters, Abell 1555 and 1558 by *Suzaku*, whose redshifts are $z = 0.127$ and 0.116 (Colafrancesco 2002). The original motivation of this observation was to examine a hypothesis that an unidentified EGRET gamma-ray source 3EGJ 1234-1318, which is located at the region of large scale filamentary structure including these two clusters (Einasto et al. 2001; Kawasaki and Totani 2002; see fig.1), is IC emission from electrons accelerated by structure forma-

tion shocks. Recently, 3EGJ 1234-1318 was detected by the new generation gamma-ray telescope *Fermi* as 1FGL J1231.1–1410, but its location has changed outside of the region of our Suzaku observation, and furthermore, its origin has been determined to be a gamma-ray pulsar (Ransom et al. 2011; Maeda et al. 2011).

However, the region around A1555 and A1558 is still interesting as a general study for a supercluster region searching for non-thermal emission clusters. There have been no targeted deep X-ray observations for these clusters. We will present the result of our search for non-thermal nature of X-ray emission, as well as a study of general physical properties of these two clusters. The Hard X-ray Detector (HXD; Kokubun et al. 2007; Takahashi et al. 2007) onboard *Suzaku* (Mitsuda et al. 2007) is characterized by its low detector background and wide field of view for hard X-rays at 10–50 keV (HXD-PIN) and 50–600 keV (HXD-GSO). *Suzaku* X-ray CCD cameras (XISs; Koyama et al. 2007) has a large effective area and a stable and low detector background in 0.5–10 keV. These detectors are suitable for observing diffuse emission from galaxy clusters.

In section 2 we present observation logs and data reduction method, and section 3 is devoted for describing the result of data analysis. In section 4 we discuss the non-thermal nature of this supercluster. We will summarize our results in section 5. Throughout this paper, the cosmological parameters of $\Omega_0 = 0.3$, $\Omega_\Lambda = 0.7$, $h = H_0/(100 \text{ Mpc}^{-1} \text{ km s}^{-1}) = 0.7$, and the baryon density parameter $\Omega_B = 0.015h^{-2}$ are assumed. Unless otherwise noted, all errors are at the 90% confidence level.

2. Observation and Data reduction

The observations were carried out on 2006 December 12-13 and 2007 December 11-12 for four pointings. Observation pointings are located along the filamentary structure and covers two galaxy clusters, A1555 and A1558. Hereafter we call these four observation areas as region 1, 2, 3, and 4, respectively (see figure 1 and figure 2). Details of the observation dates and exposure times are summarized in table 1. In latter two observations, the trouble in onboard data processing of XIS-0 occurred and no usable data was output for the half area, and therefore we do not use XIS-0 data in this study.

The data for region 1 and 2 were processed with the *Suzaku* pipeline processing of version 2.0.6.13, and region 3 and 4 were processed with the version 2.2.8.20. We used the calibration data files of 20081009, and HEASOFT version of 6.6.3. XISs data obtained with 3×3 and 5×5 edit modes for each observation and we combined them into one and applied standard filters as follows. Events with a GRADE of 0, 2, 3, 4, 6, and STATUS < 1024 were extracted. We selected good time intervals by removing the time that space craft located at the South Atlantic Anomaly (SAA) within 436 sec, the cut-off rigidity < 6.0 GV, elevation angle from the earth rim < 5°, and the sun-lit earth rim < 20°.

Major background in *Suzaku* observation is Non X-

ray Background (NXB) and Cosmic X-ray Background (CXB). NXB images and spectra of the XISs were created using the ftool “xisnxbgen” (Tawa et al. 2008). Tawa et al. (2008) studied the NXB error on a typical observation lasting for a few days. At the 90% confidence level, it is 6.7% and 12.5% for the sum of two Front Illuminated (FI) XISs (XIS-0,3) data and the Back Illuminated (BI) XIS (XIS-1) data, respectively. In the following analysis, we utilize this value as a systematic error of NXB model. The CXB fluctuation can be modeled as $\sigma_{\text{CXB}}/I_{\text{CXB}} \propto \Omega_e^{-0.5} S_c^{0.25}$ (Condon 1974). Here, Ω_e is the effective solid angle and S_c is the upper cut-off flux. From the HEAO-1 A2 results, Shafer (1983) derived $\sigma_{\text{CXB}}/I_{\text{CXB}} = 2.8\%(1\sigma)$ with $\Omega_e = 15.8 \text{ deg}^2$ and $S_c = 8 \times 10^{-11} \text{ erg s}^{-1} \text{ cm}^{-2}$. By scaling this result with XIS parameters, we obtain $\Omega_e = 0.09 \text{ deg}^2$ and $S_c \sim 4.94 \times 10^{-14} \text{ erg s}^{-1} \text{ cm}^{-2}$, which is the lowest flux of point sources detected in this observation. CXB fluctuation in XISs were estimated to be 9.65% (90% confidence limit).

The HXD data were also processed in a standard way. We screened the data with following criteria: the cut-off rigidity is larger than 6.0 GV, the elapsed time after the passage of SAA is more than 500 sec and the time before entering the SAA is more than 180 sec, elevation angle from the earth rim > 5°. We used a public NXB model provided by the HXD team for the NXB of the HXD-PIN. The version of the model is “METHOD=LCFITDT” or “tuned” (Fukazawa et al. 2009).

According to the Fukazawa et al. (2009), the NXB model reproducibility of blank sky observations separated into 10 ks exposures give distribution of 5.7% at the 90% confidence level, including the contribution from the statistical error of typically 3.3% or larger and the effect of CXB fluctuation (1.3% of the total background). Thus the systematic error of NXB model is calculated to be 4.5% at the 90% confidence level. We use the same model as Nakazawa et al. (2009) for the CXB of HXD; $N(E) = 8.7 \times 10^{-4} E^{-1.29} \times \exp(-E/40.0)$ in photons $\text{s}^{-1} \text{ keV}^{-1} \text{ FoV}^{-1}$, where E is the photon energy in keV. Details of the CXB model estimation are described in appendix 2 of Nakazawa et al. (2009). Using the same model of the CXB fluctuation with the XIS, we obtain the CXB fluctuation in HXD as 18%, with $\Omega_e = 0.32 \text{ deg}^2$ and conservative upper cut-off flux of $S_c \sim 8 \times 10^{-12} \text{ erg s}^{-1} \text{ cm}^{-2}$ in 10–40 keV band.

3. Results

3.1. HXD results

HXD-PIN detected no significant signals above the background in all regions and we only set upper limits in each observation region using 13 keV – 40 keV data. We converted residual signals (data-(NXB+CXB)) into a energy flux in 13 keV – 40 keV by assuming a power law emission with photon index $\Gamma = 2.0$ located at a center of HXD FoV. Results are summarized in table 2. Systematic errors are the sum of CXB and NXB model uncertainty as described in section 2. In all regions the residual signal is negative. It means that CXB and NXB models are slightly

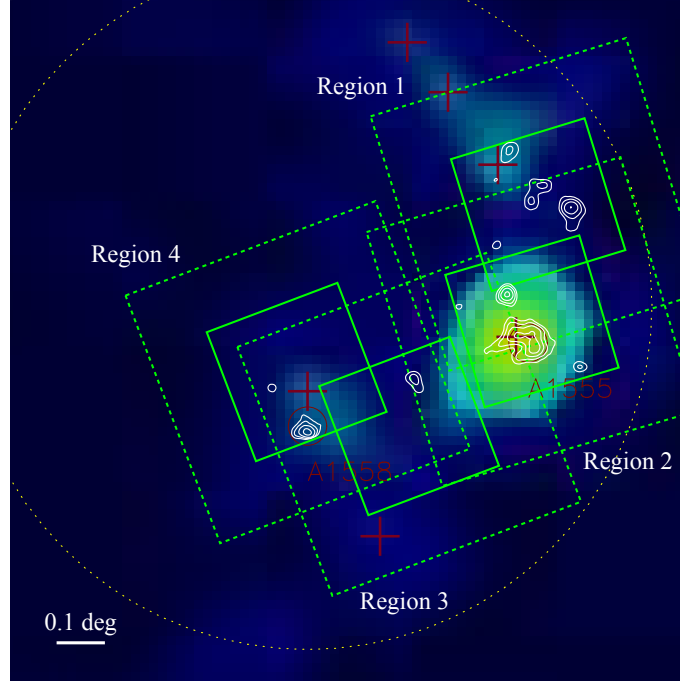


Fig. 1. The cluster “richness” map for our observation region overlaid (blue) by X-ray photon count contour (white solid line). We use the blue passband data of the APM galaxy catalog to make the “richness” map. See Kawasaki and Totani (2002) for detail. X-ray photon count contour is obtained by XIS-3 in the energy range of 0.5 – 7.0 keV. The contour levels are 2, 2.4, 2.8, 3.4, 4.0 (in 10^{-7} cts s^{-1} pix $^{-1}$). Solid and dotted green boxes are XIS and HXD FoVs, respectively. Plus signs are galaxy cluster detected by Kawasaki and Totani (2002). Dotted yellow circle represents the error circle of 3EG J1234-1318 (The location of this source has been changed by Fermi observation; see text).

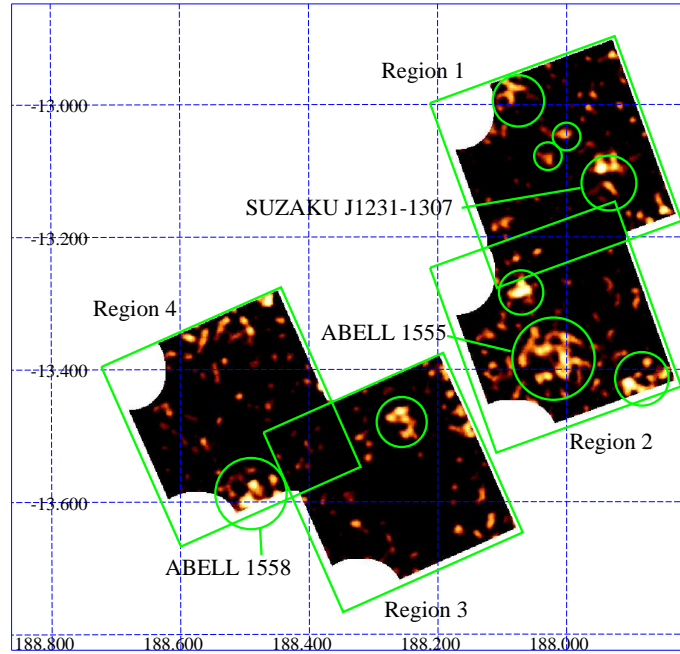


Fig. 2. XIS-3 0.5 keV – 8.0 keV mosaic image. Green boxes are XIS FoV. Images were corrected for exposure time and vignetting effect after subtracting NXB, and smoothed by a Gaussian kernel with $\sigma = 0.5$ arcmin. Small green circles show the detected sources.

Table 1. Observation log.

Obs. region	Obs. ID	Start (UT)	End (UT)	Exp. (ks)*
Region 1	801032010	Dec 12, 2006 22:16	Dec 13, 2006 18:38	25.0/18.7
Region 2	801031010	Dec 12, 2006 08:56	Dec 12, 2006 22:15	10.7/26.1
Region 3	802004010	Dec 11, 2007 01:27	Dec 11, 2007 20:30	23.2/26.3
Region 4	802005010	Dec 11, 2007 20:31	Dec 12, 2007 11:10	13.8/20.0

* The XIS/HXD Exposure time after screening

	Flux [erg cm ⁻² s ⁻¹]	Upper limit
Region 1	$(-7.4 \pm 2.3 \pm 5.9) \times 10^{-12}$	8.2×10^{-12}
Region 2	$(-0.7 \pm 2.8 \pm 6.0) \times 10^{-12}$	8.8×10^{-12}
Region 3	$(-0.1 \pm 2.4 \pm 6.0) \times 10^{-12}$	8.4×10^{-12}
Region 4	$(-0.2 \pm 2.8 \pm 6.1) \times 10^{-12}$	8.9×10^{-12}

Table 2. Measured flux and upper limits in 13 KeV – 40 keV from the HXD data. Spectral shape is assumed to be a power law with photon index 2. The former error is statistical, and the latter is systematic, due to CXB and NXB model uncertainty. All errors are at the 90% confidence level.

overestimated, and we derived the flux upper limits from statistical and systematic errors, assuming physical flux to be zero. The comparison of these limits with the expected non-thermal IC emission is discussed in section 4.1.

We also check the HXD-GSO spectrum and confirmed that it is consistent with the NXB model. Thus we did not use them.

3.2. XIS results

3.2.1. Image analysis

In figure 2, we show the XIS3 mosaic image. Images were corrected for exposure time and vignetting effect after subtracting NXB, and smoothed by a Gaussian kernel with $\sigma = 0.5$ arcmin. Diffuse emissions from A1555 and A1558 are clearly detected, which are the first detection in the X-ray band. We also selected seven circular regions centered on significant signals selected by eyes (represented by green circles in figure 2). On the other hand, there are no apparent emission associated with the filamentary structure (see figure 1).

The non-thermal diffuse emission is expected to be spatially extended. To examine whether the signals except for the A1555 and A1558 are diffuse or not, we compare the spatial expanse of these signals with the *Suzaku* point spread function (PSF). Since the PSF changes along with the source location on the XISs FoV, we estimated the PSF at the each source position using the ftool “xissim”. We simulated the image of point-like sources with the same exposure time as our observation, and utilize the spatial photon distribution of simulated point source as the PSF.

We fitted the PSF and photon distribution of observed source with a Gaussian function. If the dispersions of the PSF and the photon distribution of an observed source agreed within 1σ , we regard this source as a point like source, and otherwise we regard it as a diffuse source.

As a result, one source is determined to be diffuse (named “SUZAKU J1231-1307”, see figure 2) and others are point-like sources. We present detailed spectral analysis of this diffuse source, as well as A1555 and A1558, in next subsection.

Physical properties of all sources such as positions, photon flux, point-like or diffuse, and radio counterpart (if exists) are summarized in table 3. To derive a photon flux of a source, we assumed a power law model. Since fitting calculation is unstable when photon index is free, photon index is fixed at 2. We selected sources from NLAO VLA Sky Survey (NVSS) catalog (Condon et al. 1998) which are located within 0.3 arcmin from the source center as a radio counterpart, where 0.3 arcmin is the typical position determination accuracy of *Suzaku*. We find that SUZAKU J1231-1325 and SUZAKU J1233-1328 have a radio counterpart, NVSS J123136-132502 and NVSS J123258-132727, respectively.

3.2.2. Spectral Analysis: I. Data Reduction

We performed spectral fitting of three diffuse sources, A1555, A1558 and SUZAKU J1231-1307 to search for the non-thermal diffuse emission. For the spectral analysis of XIS data, rmf and arf files were created using *Suzaku* ftool “xisrmfgen” and “xissimarfgen”, respectively. Two XIS-FI (XIS0, XIS3) spectra and response files for each sources are summed up, and XIS-FI and XIS-BI (XIS1) spectra are fitted simultaneously. Energy band used in the spectral analysis is 0.5 – 7.0 keV.

The background spectrum of each FoV were modelled as follows. First, we extracted the spectrum from the whole FoV and subtracting the sources and NXB, and then performed spectral fitting of this data with the CXB model. For the CXB model, we used a model including a power-law component with a fixed photon index $\Gamma = 1.4$, a fixed temperature (0.08 keV) thermal component, and another thermal component whose temperature is a fitting parameter around 0.3 keV (the so-called “Galactic components”). The power-law component suffers from Galactic absorption, and it was modeled by the *wabs* code. For the N_{H1} column density we use the value of Kalberla et al. (2005), which are 3.47, 3.41, 3.41 and $3.43 \times 10^{20} \text{ cm}^{-2}$ for the regions 1, 2, 3 and 4, respectively.

Results of spectral fittings to CXB are summarized in table 4, where the values of fitting model parameters (the three normalization parameters and a fitting temperature) are shown. In each region, our CXB model describes the observed data well (see the reduced χ^2 in the table), and the 2-10 keV fluxes of the power-law component are consistent within 90% statistic and systematic

Table 3. The list of sources which are detected in this observation. See the text for detail.

Name	RA	DEC	Flux *	Point/Diffuse	Counter part
SUZAKU J1232-1259	12:32:18	−12:59:41	1.4 ± 0.20	Point	—
SUZAKU J1232-1302	12:32:00	−13:02:55	0.62 ± 0.13	Point	—
SUZAKU J1232-1304	12:32:07	−13:04:42	0.49 ± 0.12	Point	—
SUZAKU J1231-1307	12:31:44	−13:07:08	—	Diffuse	—
SUZAKU J1232-1317	12:32:17	−13:17:02	1.0 ± 0.19	Point	—
SUZAKU J1231-1323 (A1555)	12:31:60	−13:23:33	—	Diffuse	—
SUZAKU J1231-1325	12:31:30	−13:25:00	0.78 ± 0.28	Point	NVSS J123136-132502
SUZAKU J1233-1328	12:33:02	−13:28:46	0.65 ± 0.24	Point	NVSS J123258-132727
SUZAKU J1234-1334 (A1558)	12:34:00	−13:34:32	—	Diffuse	—

* Energy flux in 10^{-13} erg s $^{-1}$ cm $^{-2}$, where errors are at the 90% confidence limit. Flux of three diffuse sources are shown in table 5.

error with the best-fit value derived using *ASCA*, which is $5.67 \pm 0.04 \times 10^{-8}$ erg cm $^{-2}$ s $^{-1}$ str $^{-1}$ (Kushino et al. 2002). It has been known that solar-wind charge exchange with H I in the Earth’s geocorona accounts for a part of X-ray background below 1keV (e.g., Cravens 2000; Fujimoto et al. 2007). We do not consider detailed characterization of this component in this paper since our CXB model well describes the spectra of background regions. (Note that this component may be implicitly included in the modeling of the Galactic component.)

Then, we simulated the CXB spectrum to produce X-ray counts using the obtained parameters of the CXB and arf files at each source position. Finally, we combined the simulated CXB and NXB spectrum, and utilized it as a background spectrum in the spectral fitting of sources.

3.2.3. Spectral Analysis II. Model Fittings

We fitted the spectra of the three diffuse sources by thermal, power-law, and thermal plus power-law models. For the thermal model we use the *apev* code in the XSPEC (v11.3.2). For the value of N_{HI} column density we also used the value of Kalberla et al. (2005), which are 3.49, 3.41, and 3.43×10^{20} cm $^{-2}$ for A1555, A1558 and SUZAKU J1231-1307, respectively. Since the statistics is limited we could not determine the metal abundance by spectral fitting, and therefore we fixed it at 0.3 Z_{\odot} which is the average value of the clusters in the distant cluster catalog compiled by Ota & Mitsuda (2004). We adopted the solar abundance table of Anders & Grevesse (1989). The redshift was fixed at $z = 0.127$ for A1555 and $z = 0.116$ for A1558, respectively (Colafrancesco 2002). For the SUZAKU J1231-1307 we fixed the redshift at 0.1, since fitting is unstable when redshift is set to free due to low statistics. Then the free parameters are the normalizations of the thermal and power-law components, temperature, and photon index. The results of spectral fittings are summarized in table 5, and the spectra are shown in figure 3, 4, 5, respectively.

As a result, all the three models are consistent with the data of all the three sources in terms of the value of χ^2 , except the power-law model against A1558 (5% probability of getting such a large χ^2). However, in the case of A1555 the fit significantly improves when we fit by the thermal plus power-law model ($\chi^2/\text{d.o.f} = 27.8/44$), com-

pared with the pure thermal model (42.4/46). The F-test probability is 9.3×10^{-5} , indicating that the former is significantly favored than the latter. We examined the sensitivity of this result to the CXB fluctuation, by artificially increasing the CXB flux by 14.8%, which is 1σ of the fluctuation (see section 2 for detail). The resultant F-test probability only slightly increases to 4.2×10^{-4} . We will discuss implications of those results in §4.1.

In contrast, the spectrum of A1558 was not well fitted by the power law model, and χ^2 value did not improve when we fit by the thermal plus power-law model, compared with the pure thermal model. Therefore A1558 seems to be a well relaxed cluster.

The spectrum of unknown diffuse source SUZAKU J1231-1307 is well fitted with all models. We will discuss this object later (see section 4.1).

3.3. Total Mass estimation of A1555

Here we present a detailed estimation of the total mass of A1555, M_{tot} , because this source has been detected with the highest significance and the whole cluster is included in the field of view.

In the isothermal β -model (Cavaliere & Fusco-Femiano 1976), the radial profile of X-ray surface brightness is written as

$$S_x(b) = S_0 \left[1 + \left(\frac{b}{r_c} \right)^2 \right]^{-3\beta+1/2}, \quad (1)$$

where b , S_0 , r_c and β are the projected radius, central surface brightness, core-radius and the outer slope of density profile, respectively.

We simulated the thermal emission from A1555 which follows β model profile using the ftool “xissim”, and compare it with the observation to estimate the value of β and r_c . As a spectral model, we used a single temperature thermal model with the parameters listed in table 5.

In figure 6, we show the observed surface brightness profile of A1555 with the results of simulations. First, we simulated with $\beta=0.5$ and $r_c=0.16$ Mpc (shown as “single β model” in figure 6). This value of r_c is an average of the clusters located at $z = 0.1 - 0.15$ in the distant cluster

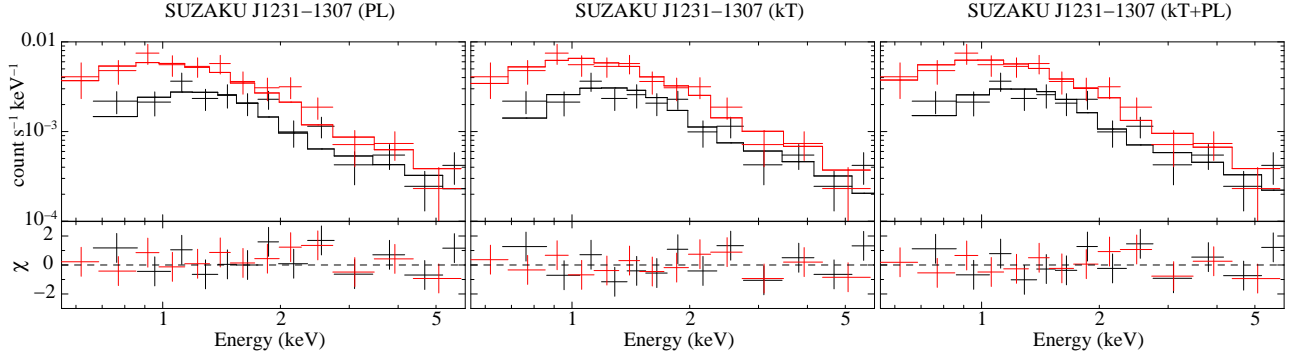


Fig. 3. Spectrum of diffuse source, SUZAKU J1231-1307 with the power law model, thermal model, and thermal + power law model (left to right). Data points of XIS-FI are represented by black, while XIS-BI by red. Solid line represents best-fit model. See Table 5 for fitted model parameters.

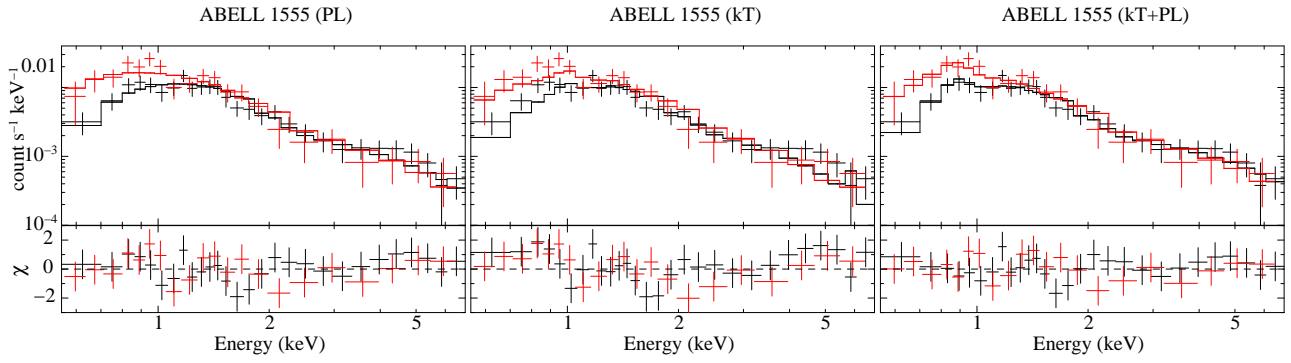


Fig. 4. The same as figure 3, but for Abell1555.

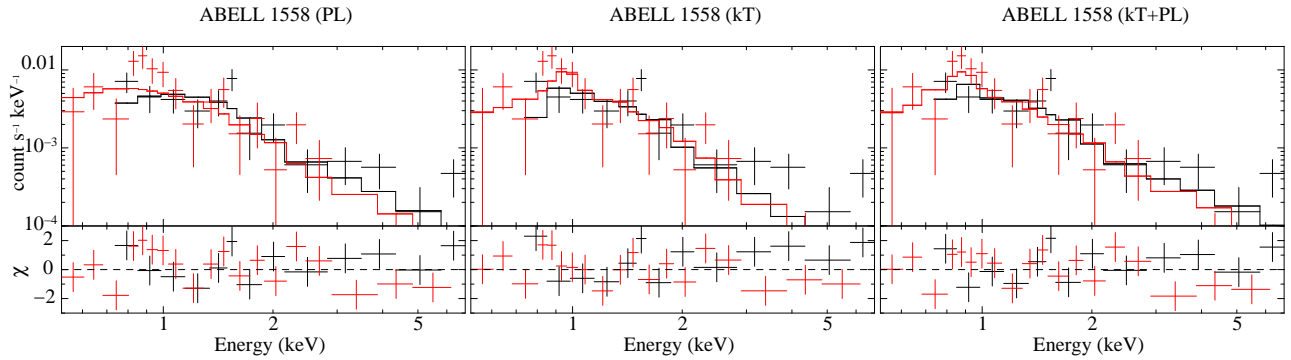


Fig. 5. The same as figure 3, but for Abell 1558.

Table 4. The best fit parameters of the CXB model for background spectrum. All errors are given at the 90% confidence limit.

	F_{PL}^*	N_{cool}^\dagger	N_{hot}^\dagger	$kT_{\text{hot}}^\parallel$	$\chi^2/\text{d.o.f}$
Region 1	$5.3^{+0.3}_{-0.3}$	$1.2^{+0.4}_{-0.3}$	$4.7^{+1.7}_{-1.1}$	$0.26^{+0.03}_{-0.03}$	110.1/96
Region 2	$5.8^{+0.3}_{-0.3}$	$1.3^{+0.3}_{-0.3}$	$7.4^{+1.6}_{-1.4}$	$0.29^{+0.03}_{-0.03}$	93.6/121
Region 3	$5.2^{+0.3}_{-0.3}$	$1.4^{+0.3}_{-0.4}$	$6.3^{+1.6}_{-1.1}$	$0.28^{+0.03}_{-0.03}$	137.7/116
Region 4	$5.1^{+0.4}_{-0.4}$	$1.5^{+0.4}_{-0.4}$	$5.4^{+1.6}_{-1.4}$	$0.29^{+0.05}_{-0.04}$	120.5/105

* Surface brightness of power law component in 2.0 – 10.0 keV (in $10^{-8} \text{ erg cm}^{-2} \text{ s}^{-1} \text{ str}^{-1}$).

† Normalization in the thermal model, for the cooler and hotter galactic thermal components (in 10^{-2} cm^{-5} and 10^{-4} cm^{-5} , respectively).

‖ Temperature of the hotter galactic thermal component (in keV).

Table 5. The best fit parameters of the thermal, power-law (PL), and thermal plus PL model for the three diffuse sources: SUZAKU J1231-1307, A1555 and A1558. All errors are at the 90% confidence limit.

Object	Model	N_{th}^*	kT^\dagger	F_{PL}^\ddagger	Γ^\S	$\chi^2/\text{d.o.f}$
SUZAKU J1231-1307	Thermal	$0.9^{+0.2}_{-0.2}$	$3.7^{+2.3}_{-1.1}$	—	—	15.3/23
	PL	—	—	$6.5^{+2.3}_{-1.9}$	$1.9^{+0.26}_{-0.24}$	18.5/23
	Thermal+PL	$1.0^{+0.4}_{-0.8}$	$6.3^{+5.6}_{-5.6}$	$1.6^{+7.6}_{-1.6}$	2.0 (fixed)	16.9/22
A1555	Thermal	$3.0^{+0.3}_{-0.3}$	$2.0^{+0.54}_{-0.33}$	—	—	42.4/46
	PL	—	—	$10.0^{+2.8}_{-2.4}$	$2.5^{+0.22}_{-0.20}$	33.0/46
	Thermal+PL	$0.8^{+0.9}_{-0.6}$	$1.1^{+0.39}_{-0.22}$	$10.0^{+3.6}_{-3.4}$	$2.2^{+0.33}_{-0.46}$	27.8/44
A1558	Thermal	$1.6^{+0.4}_{-0.5}$	$1.4^{+0.31}_{-0.27}$	—	—	37.3/29
	PL	—	—	$4.8^{+2.7}_{-2.0}$	$2.7^{+0.43}_{-0.37}$	46.7/29
	Thermal+PL	$1.4^{+0.6}_{-0.4}$	$1.3^{+0.42}_{-0.27}$	$1.0^{+4.3}_{-1.0}$	2.0 (fixed)	37.1/27

* Normalization of the thermal model (in 10^{-4} cm^{-5}).

† Temperature (in keV).

‡ Flux of power law component. (in $10^{-14} \text{ erg cm}^{-2} \text{ s}^{-1}$ over the energy range 2.0 – 10.0 keV)

§ Photon index of power law component

catalog (Ota and Mitsuda 2004). The dispersion of r_c is about factor two, and we confirmed that this uncertainty of r_c does not significantly affect the estimation of the total cluster mass (about factor 0.5). The value of β is selected to fit the observation. This value is in agreement with the average of the distant clusters (Ota and Mitsuda 2004). It can be seen that the simulation well reproduces the observed surface brightness profile at the region except the central two data points.

The central excess is often represented by an additional small scale β -model component (double- β model; Jones & Forman 1984). We therefore performed a simulation by adding a small scale component of $r_c = 10 \text{ kpc}/h$ and $\beta = 0.7$, in addition to the single β model used above, as a test of the double β model. Those values of r_c and β are averaged values of the small scale components in Mulchaey and Zabludoff (1998). The simulation result is shown in figure 6. The double β model gives a better fit, but is still discrepant with the innermost data by about two sigma. This may be just a statistical fluctuation, or may indicate a contribution from a AGN. Since it is difficult to further discuss the origin of this excess due to the low statistics of our data and limitation of spatial resolution of *Suzaku*, we conservatively consider a systematic error of a factor of about 2 for β , from the dispersion of β in the distant

cluster sample of Ota & Mitsuda (2004).

Under the isothermal β model and also assuming that the cluster gas is in hydrostatic equilibrium, we can estimate the total cluster mass from the value of r_c , β , and gas temperature (Cavaliere & Fusco-Femiano 1976). Using the single β model with $\beta = 0.5$ and $r_c = 0.16 \text{ Mpc}$, $M_{\text{tot}}(< r_{500})$ is estimated to be $7.43^{+4.1+14.5}_{-2.2-5.0} \times 10^{13} M_\odot$ and $r_{500} = 0.69^{+0.11+0.3}_{-0.10-0.2} \text{ Mpc}$, where the r_{500} is a radius where the ratio of total cluster mass density to critical density became 500. In the above mass estimation we used the value of gas temperature as $2.0^{+0.54}_{-0.33} \text{ keV}$ which is derived from the single thermal component fit (see table 5). If we used the temperature derived from the thermal+PL fit, $1.1^{+0.39}_{-0.22} \text{ keV}$, and the same value of β and r_c assuming that thermal and non-thermal component have the same radial profile, $M_{\text{tot}}(< r_{500})$ becomes $2.8^{+1.7+5.8}_{-0.8-2.0} \times 10^{13} M_\odot$. The former errors in M_{tot} and r_{500} are statistical, simply estimated from statistical errors of kT and β , while the latter ones are systematic, estimated from the systematic error of β . The value of total cluster mass and temperature are consistent with the known correlation between the total cluster mass and temperature (e.g., Ota and Mitsuda 2004).

If we adopt the double β model, the total cluster mass becomes $7.43 \times 10^{13} M_\odot$ (with thermal model) or

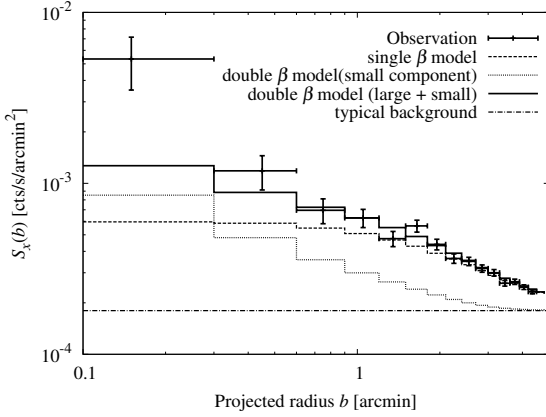


Fig. 6. The surface brightness profile of Abell 1555. The crosses are XIS-BI data. The dashed line represents best-fit single β model. The solid line denotes double β model while the dotted line is small scale component double- β model. The typical background level has shown by dot-dashed line.

$2.8 \times 10^{13} M_{\odot}$ (with thermal + PL model). The difference between the mass estimated with single β model and double β model is less than 1%.

In the above mass estimation, we assumed that A1555 is isothermal. We checked the effect of this assumption on the mass estimation by comparing the total cluster mass of several clusters estimated by Fukazawa et al. (2004) with the total cluster mass estimated by Vikhlinin et al. (2006), where the former assumed isothermal while the latter did not. These two differ by $\sim 20\%$, indicating a similar level of systematic errors for our mass estimates.

We also derive a luminosity of A1555 in 0.2 – 10.0 keV band from spectral fitting with thermal model. It is estimated to be $8.8 \pm 1.6 \times 10^{43}$ erg s $^{-1}$.

4. Discussion

4.1. On the Evidence for Non-thermal Emission from A1555

Here we discuss the origin of the non-thermal emission implied for A1555. First we discuss the possibility that it is due to the IC scattering of CMB photons by accelerated electrons. From the $\Gamma = 2.2$ power-law component of the thermal+PL fit for A1555, we estimate the total energy of non-thermal electrons to be $3.1^{+1.1}_{-1.1} \times 10^{59}$ erg assuming $z = 0.127$, in the electron energy range 0.4–1.5 GeV corresponding to the X-ray energy range of 0.5–7.0 keV. The total thermal energy of baryon gas when the structure formation occur is given by $E_{\text{baryon}} \sim (3/4)(\Omega_B/\Omega_0)M_{\text{tot}}V_c^2$, where V_c is circular velocity of the halo, and which can be calculated from spherical collapse model (Peebles 1980; Kitayama and Suto 1996) which is widely used in study of structure formation. If we use the total mass of A1555 estimated with $kT = 1.1$ keV from the thermal+PL fit (see section 3.3) E_{baryon} becomes $7.0^{+8.5+15.0}_{-3.1-4.8} \times 10^{60}$ erg, where the former error is statistic while the latter is systematic which are estimated from the uncertainty of total mass (see section 3.3 for detail). Therefore the fraction of

non-thermal electron energy becomes $\xi_e \sim 0.044$, which is consistent with the typical value discussed in the literature (e.g., Fusco-Femiano et al. 1999, but see also Rossetti & Molendi 2004).

From the flux of non-thermal PL component and the strength of magnetic field, B , we can estimate the flux of possible synchrotron emission due to the same electron population which emits the non-thermal IC emission. As already noted in section 3.2.1, A1555 has no radio counter part in NVSS catalog. Flux limit of NVSS is 2.5 mJy/beam and beam size is 45". Assuming that the synchrotron emission has the same spectral index with the PL component, $\Gamma = 2.2$, and extended about 1 Mpc, the expected brightness at 1.4 GHz is estimated to be 2.2 mJy/beam with $B = 1 \mu\text{G}$. The typical value of B is 0.1 – 1 μG , and therefore the scenario of non-thermal IC emission is not inconsistent with the radio observation.

We also discuss the detectability of the non-thermal IC emission with *Fermi* Large Area Telescope (Atwood et al. 2009). Theoretically it is reasonable to expect that the IC emission extends to the GeV energy band with a photon index of $\Gamma \sim 2$ (e.g., Totani & Kitayama 2000). Extrapolating from the observed X-ray flux, the expected flux in the energy higher than 100 MeV became $F_{>100\text{MeV}} = 3.9 \times 10^{-10}$ and 4.4×10^{-11} photons cm $^{-2}$ s $^{-1}$ for $\Gamma = 2.0$ and 2.2, respectively. These fluxes are about one order of magnitude lower than the sensitivity of *Fermi*, and the *Fermi* observation does not give a strong constraint.

It should also be noted that the flux of power law component in 13.0 – 40.0 keV is consistent with the flux upper limit obtained by HXD analysis.

It has been known that relaxed clusters do have a cool core and a radially decreasing temperature at large radii, and merging clusters have shock heated structures. To approximate these effects on our results we fitted the two temperature thermal model to the spectrum of A1555. The fitting results are summarized in table 6. The fit also significantly improves comparing with the single temperature fit. The thermal+PL model has a smaller χ^2 value than the two temperature model, but the likelihood ratio is just a factor of about four. Therefore the two temperature model provides another good description of the data, as an alternative to the thermal+PL model. The two temperatures are determined to be $1.0^{+0.34}_{-0.28}$ keV and $3.6^{+4.5}_{-2.1}$ keV, which are similar to the result of two temperature analysis of the Virgo and Centaurus cluster (Fukazawa et al. 2000).

We also check a possibility that the origin of the power-law component is the background (or foreground) AGNs. We found two radio point sources at the outer region of A1555, NVSS J1232-1323 and NVSS 1232-1321 (Condon et al. 1998). Their flux density at 1.4 GHz are 7.0 ± 0.5 (NVSS J1232-1323) and 4.0 ± 0.6 (NVSS J1232-1321) mJy. If we extrapolate their flux to the X-ray regime using the spectral energy distribution model of AGNs constructed by Elvis et al. (1994), the expected flux become $0.8 \times 10^{-14} - 1.0 \times 10^{-12}$ erg s $^{-1}$ cm $^{-2}$ in 2.0–10.0 keV. The estimated flux of PL component in the spectrum of A1555

is $1.0 \times 10^{-13} \text{ erg s}^{-1} \text{ cm}^{-2}$ in 2.0–10.0 keV, and therefore the X-ray flux extrapolated from the flux of radio sources are consistent with the flux of PL component within the uncertainty. In conclusion we can not reject the scenario that a AGN explains the non-thermal component in the spectrum of A1555.

4.2. On SUZAKU J1231-1307

We also detected interesting diffuse object, SUZAKU J1231-1307, which locates along the large scale filamentary structure. The spectrum of SUZAKU J1231-1307 is well fitted by power-law, thermal, and thermal + PL model with similar χ^2 value. If SUZAKU J1231-1307 is a galaxy cluster, the temperature is 3.7 keV and the total cluster mass is estimated to be $2.6_{-1.0}^{+2.7} \times 10^{14} M_{\odot}$. Here we used the correlation between the total mass and temperature obtained by Vikhlinin et al. (2009). If the PL component really exists, the total energy of non-thermal electron becomes $5.0_{-5.0}^{+23.6} \times 10^{58} \text{ erg}$, which is about 15% of A1555. Further observation is required to determine the origin of this mysterious object.

4.3. IC emission upper-limit associated with the large-scale structure as a whole

If the non-thermal IC emission is emitted from the whole region of the large scale filamentary structure and extended more than XIS FoV, the flux of this emission has some contribution to the background flux. From the error estimation of CXB flux, we derive an upper limit to this component. As already noted in section 2, the systematic error of CXB flux in one XIS FoV is estimated to be 9.65%. Combining this uncertainty with the statistical error in CXB estimation (see table 4), total uncertainty of the CXB emission from all XIS FoV becomes 5.4%. From this uncertainty and the average value of CXB surface brightness, the upper limit on the surface brightness of non-thermal IC emission is estimated to be $2.9 \times 10^{-9} \text{ erg cm}^{-2} \text{ s}^{-1} \text{ str}^{-1}$. The total FoV of four XISs is $1.1 \times 10^{-4} \text{ str}$, and therefore the flux upper limit of non-thermal IC emission becomes $3.2 \times 10^{-13} \text{ erg cm}^{-2} \text{ s}^{-1}$. This limit is in the same order of magnitude as the flux of power-law component in the spectrum of A1555, $1.0 \times 10^{-13} \text{ erg cm}^{-2} \text{ s}^{-1}$.

5. Summary

We performed the deepest X-ray observation of the supercluster region including A1555 and A1558 with *Suzaku*. This region is interesting since large scale filamentary structures connected with the two galaxy clusters exist, but only RASS data was available in the X-ray band.

We have detected the two galaxy clusters A1555 and A1558 for the first time in the X-ray band. Six point sources and one diffuse source (SUZAKU J1231-1307) were also detected. The total mass of A1555 was derived using the beta model. We examined the non-thermal nature of SUZAKU J1231-1307, A1555, and A1558, and there are no evidence for non-thermal emission for SUZAKU J1231-1307 and A1558. However, we found

that the A1555 spectrum cannot be fit by one-temperature thermal model. A thermal plus power-law model significantly improves the fit, and if this power-law component is the IC emission of CMB photons, the non-thermal electron energy is estimated to be 2% of the thermal energy of the cluster, which is similar to the values often discussed in the literature for galaxy clusters.

However, the A1555 spectrum can also be fit by a two-temperature thermal model, and the possibility of underlying AGNs cannot be excluded. More detailed and sensitive observational studies are desired for better understanding of this interesting region.

This work was supported by the Grant-Aid for the Global COE Program “The Next Generation of Physics, Spun from University and Emergenc” from the Ministry of Education, Culture, Sports, Science and Technology (MEXT) of Japan. TT and KN was supported in part by the Grant-in-Aid (22244019) and Grant-in-Aid (18104004), respectively, for Scientific Research from MEXT.

References

- Ackermann, M., et al. 2010, ApJ, 717, L71
- Aharonian, F. A., et al. 2009a, A&A, 495, 27
- Aharonian, F. A., et al. 2009b, A&A, 502, 437
- Aleksic, J. (The MAGIC Collaboration), Pfrommer, C., Pinzke, A., Ensslin, T. A., Inoue, S., & Ghisellini, G. 2010, ApJ, 710, 634
- Anders, E., & Grevesse, N. 1989, Geochim. Cosmochim. Acta, 53, 197
- Atwood, W. B., et al. 2009, ApJ, 697, 1071
- Blasi, P., Gabici, S., & Brunetti, G. 2007, IJMPA, 22, 681
- Cavaliere, A., & Fusco-Femiano, R. 1978, A&A, 70, 677
- Colafrancesco, S. 2002, A&A, 396, 31
- Condon, J. J. 1974, ApJ, 188, 279
- Condon, J. J., Cotton, W. D., Greisen, E. W., Yin, Q. F., Perley, R. A., Taylor, G. B., & Broderick, J. J., 1998, AJ, 115, 1693
- Cravens, T. E. 2000, ApJ, 532, L153
- Einasto, M., Einasto, J., Tago, E., Möller, V., & Andernach, H. 2001, AJ, 122, 2222
- Elvis, M., et al. 1994, ApJS, 95, 1
- Feretti, L. 2005, Advances in Space Research, 36, 729
- Fujimoto, R., et al. 2007, PASJ, 59, 133
- Fukazawa, Y., Makishima, K., Tamura, T., Nakazawa, K., Ezawa, H., Ikebe, Y., Kikuchi, K., & Ohashi, T. 2000, MNRAS, 313, 21
- Fukazawa, Y., Makishima, K., & Ohashi, T. 2004, PASJ, 56, 965
- Fukazawa, Y., et al. 2009, PASJ, 61, S17
- Fusco-Femiano, R., Dal Fiume, D., Feretti, L., Giovannini, G., Grandi, P., Matt, G., Molendi, S., & Santangelo, A. 1999, ApJ, 513, L21
- Fusco-Femiano, R., Orlandini, M., Brunetti, G., Feretti, L., Giovannini, G., Grandi, P., & Setti, G. 2004, ApJ, 602, L73
- Fusco-Femiano, R., Landi, L., & Orlandini, M. 2007, ApJ, 654, L9
- Giovannini, G., & Feretti, L., 2000, New Astronomy, 5, 335
- Govoni, F., Feretti, L., 2004, Int.J.Mod.Phys., D13, 1549

Table 6. Best fit parameters of two-temperature thermal model fitted to the A1555. All errors are at the 90% confidence limit.

kT_{low}^*	N_{low}^\dagger	kT_{hi}^*	N_{hi}^\dagger	$\chi^2/\text{d.o.f}$
$1.0^{+0.3}_{-0.3}$	$0.9^{+1.2}_{-0.5}$	$3.6^{+4.5}_{-2.1}$	$1.9^{+0.6}_{-1.2}$	30.6/44

* Temperature of cooler (hotter) component (in keV).

† Normalization of the *apec* code, for cooler and hotter component (in 10^{-4} cm^{-5}).

- Jones, C., Forman, W. 1984, ApJ, 276, 38
 Kalberla, P. M. W., et al. 2005, A&A, 440, 775
 Kawasaki, W., & Totani, T. 2002, ApJ, 576, 679
 Kokubun, M., et al. 2007, PASJ, 59, S53
 Koyama, K., et al. 2007, PASJ, 59, S23
 Kushino, A., Ishisaki, Y., Morita, U., Yamasaki N. Y.,
 Ishida, M., Ohashi, T., & Ueda, Y. 2002, PASJ, 54, 327
 Maeda, K., et al. 2011, ApJ, 729, 103
 Makishima, K., et al. 2001, PASJ, 53, 401
 Mitsuda, K., et al. 2007, PASJ, 59, S1
 Mulchaey, J. S., & Zabludoff, A. I. 1998, ApJ, 496, 73
 Nakazawa, K., et al. 2009, PASJ, 61, 339
 Ota, N., & Mitsuda, K. 2004, A&A, 428, 757
 Ransom, S. M., et al. 2011, ApJ, 727, L16
 Rossetti, M., & Molendi, S. 2004, A&A, 414, 41
 Shafer, R. A. 1983, PhD thesis, University of Maryland
 Takahashi, T., et al. 2007, PASJ, 59, S35
 Tawa, N., et al. 2008, PASJ, 60, 11
 Vikhlinin, A., et al. 2006, ApJ, 640, 691
 Vikhlinin, A., et al. 2009, ApJ, 692, 1033
 Wik, D. R., Sarazin, C. L., Finoguenov, A., Matsushita, K.,
 Nakazawa, K., & Clarke, T. E. 2009, ApJ, 696, 1700
 Willson, M. A. G. 1970, MNRAS, 151, 1